

Demonstration of Athena X-IFU Compatible 40-Row Time-Division-Multiplexed Readout

Malcolm Durkin^{ID}, Joseph S. Adams, Simon R. Bandler, James A. Chervenak, Saptarshi Chaudhuri, Carl S. Dawson, Edward V. Denison, William B. Doriese^{ID}, Shannon M. Duff, Fred M. Finkbeiner^{ID}, Connor T. FitzGerald, Joseph W. Fowler, Johnathon D. Gard, Gene C. Hilton, Kent D. Irwin, Young Il Joe, Richard L. Kelley, Caroline A. Kilbourne^{ID}, Antoine R. Miniussi, Kelsey M. Morgan^{ID}, Galen C. O’Neil, Christine G. Pappas, Frederick S. Porter, Carl D. Reintsema, David A. Rudman, Kazuhiro Sakai, Stephen J. Smith, Robert W. Stevens, Daniel S. Swetz, Paul Szypryt, Joel N. Ullom, Leila R. Vale, Nicholas A. Wakeham^{ID}, Joel C. Weber, and Betty A. Young

Abstract—Time-division multiplexing (TDM) is the backup readout technology for the X-ray Integral Field Unit (X-IFU), a 3168-pixel X-ray transition-edge sensor (TES) array that will provide imaging spectroscopy for European Space Agency’s Athena satellite mission. X-IFU design studies are considering readout with a multiplexing factor of up to 40. We present data showing 40-row TDM readout (32 TES rows + 8 repeats of the last row) of TESs that are of the same type as those being planned for X-IFU, using measurement and analysis parameters within the ranges specified for X-IFU. Single-column TDM measurements have best-fit energy resolution of (1.91 ± 0.01) eV for the Al K α complex (1.5 keV), (2.10 ± 0.02) eV for Ti K α (4.5 keV), (2.23 ± 0.02) eV for Mn K α (5.9 keV), (2.40 ± 0.02) eV for Co K α (6.9 keV), and (3.44 ± 0.04) eV for Br K α (11.9 keV). Three-column measurements

Manuscript received October 27, 2018; accepted March 8, 2019. Date of publication March 19, 2019; date of current version April 23, 2019. This work was supported by the NASA SAT program, “Providing Enabling & Enhancing Technologies for a Demonstration Model of the Athena X-IFU.” (Corresponding author: Malcolm Durkin.)

M. Durkin, E. V. Denison, W. B. Doriese, S. M. Duff, J. W. Fowler, J. D. Gard, G. C. Hilton, Y. I. Joe, K. M. Morgan, G. C. O’Neil, C. G. Pappas, C. D. Reintsema, D. A. Rudman, R. W. Stevens, D. S. Swetz, P. Szypryt, J. N. Ullom, L. R. Vale, and J. C. Weber are with the National Institute of Standards and Technology, Boulder, CO 80305 USA (e-mail: malcolm.durkin@nist.gov; ed.denison@nist.gov; william.doriese@nist.gov; shannon.duff@nist.gov; joe.fowler@nist.gov; johnathan.gard@nist.gov; gene.hilton@nist.gov; youngil.joe@nist.gov; kelsey.morgan@nist.gov; galen.oneil@nist.gov; christine.pappas@nist.gov; carl.reintsema@nist.gov; david.rudman@nist.gov; robert.stevens@nist.gov; daniel.swetz@nist.gov; paul.szypryt@nist.gov; joel.ullom@nist.gov; leila.vale@nist.gov; joel.weber@nist.gov).

J. S. Adams, S. R. Bandler, J. A. Chervenak, F. M. Finkbeiner, R. L. Kelley, C. A. Kilbourne, A. R. Miniussi, F. S. Porter, K. Sakai, S. J. Smith, and N. A. Wakeham are with the National Aeronautics and Space Administration, Greenbelt, MD 20771 USA (e-mail: joseph.s.adams@nasa.gov; simon.r.bandler@nasa.gov; james.a.chervenak@nasa.gov; fred.m.finkbeiner@nasa.gov; richard.l.kelley@nasa.gov; caroline.a.kilbourne@nasa.gov; antoine.r.miniussi@nasa.gov; frederick.s.porter@nasa.gov; kazuhiro.sakai@nasa.gov; stephen.j.smith@nasa.gov; nicholas.a.wakeham@nasa.gov).

S. Chaudhuri, C. S. Dawson, and K. D. Irwin are with the Department of Physics, Stanford University, Stanford, CA 94305 USA (e-mail: schaudh2@stanford.edu; csdawson@stanford.edu; irwin@stanford.edu).

B. A. Young is with the Department of Physics, Stanford University, Stanford, CA 94305, USA, and also with the Department of Physics, Santa Clara University, Santa Clara, CA 95053 USA (e-mail: bayoung@stanford.edu).

C. T. FitzGerald is with the Department of Physics, Santa Clara University, Santa Clara, CA 95053 USA (e-mail: cfitzgerald@scu.edu).

Color versions of one or more of the figures in this paper are available online at <http://ieeexplore.ieee.org>.

Digital Object Identifier 10.1109/TASC.2019.2904472

have best-fit resolution of (2.03 ± 0.01) eV for Ti K α and (2.40 ± 0.01) eV for Co K α . The degradation due to the multiplexed readout ranges from 0.1 eV at the lower end of the energy range to 0.5 eV at the higher end. The demonstrated performance meets X-IFU’s energy-resolution and energy-range requirements. True 40-row TDM readout, without repeated rows, of kilopixel scale arrays of X-IFU-like TESs is now under development.

Index Terms—Transition-edge sensors, superconducting quantum interference devices, multiplexed readout, athena satellite.

I. INTRODUCTION

Due to their combination of high collecting efficiency [1] and high energy-resolution [2], arrays of transition-edge-sensor (TES) microcalorimeters are candidates for deployment in next-generation X-ray observatories. The Athena X-ray Integral Field Unit (X-IFU) [3] will use a 3,168 pixel TES array to perform imaging X-ray spectroscopy at energies up to 12 keV with stringent energy resolution requirements: 2 eV resolution below 1 keV, 2.5 eV resolution between 1 keV and 7 keV, and 5 eV resolution above 10 keV. Practical readout of kilopixel (1000 pixels) scale TES arrays requires multiplexed readout, especially in a satellite mission with strict limits on power, wire count, and mass. Frequency-division multiplexing is the primary [4] and time-division multiplexing (TDM) is the backup readout option for X-IFU.

TDM is a mature technology that is routinely deployed in 250-pixel scale TES X-ray microcalorimeter spectrometers, using 8-column by ≤ 32 -row readout, in beamline and table-top measurement systems [5]. In our TDM architecture [6], shown in Fig. 1, each dc-biased TES has a corresponding first-stage superconducting quantum interference device (SQUID) ammeter (SQ1). The SQ1s are activated one at a time via a flux-actuated superconducting switch [7], so the TESs in a readout column are measured sequentially within a readout frame. SQ1 signals are then amplified by a SQUID series array (SSA) and digitized by room-temperature electronics. In this scheme, every SQ1 activation is called a *row* and a full set of samples of a column is a *frame*. TDM columns are read out in parallel. X-IFU will require row and column counts beyond the present state of the art in X-ray-TES-array readout.

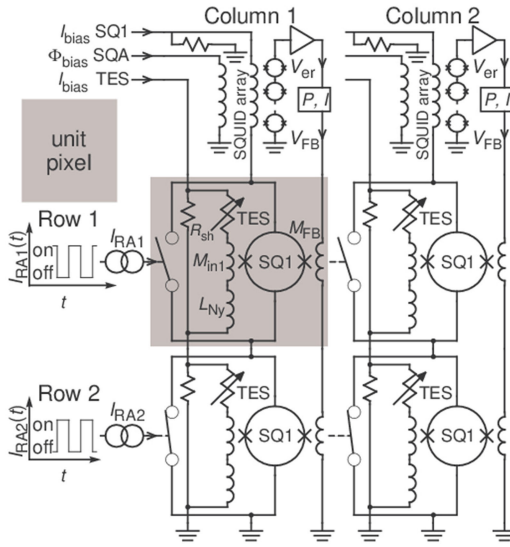


Fig. 1. Schematic of 2-column \times 2-row TDM. Each dc-biased TES is read out by a first stage SQUID amplifier (SQ1) via inductive coupling (M_{in1}). A row of SQ1s is turned on by applying a row address current (I_{RA}) to the corresponding row address line, opening the row's flux actuated switches. During TDM operation, rows are opened sequentially, reading out one TES per column at a time. Each column's SQ1 signals are passed to a SQUID series array amplifier, whose voltage (V_{er}) is read out by room temperature electronics. To achieve the timing and noise of 40-row TDM with only 32 physical row addresses, we repeated the final row 8 times, but did not include data from repeated rows in analysis. This schematic is published concurrently in these proceedings by Doriese *et al.* [6].

II. 40-Row TDM READOUT

The 40-row-TDM experiments described here were performed in a pair of 8-column \times 32-row systems [5]. The Al $K\alpha$ measurements were acquired at NASA, while the rest of the spectra were acquired at NIST. The two 8-column \times 32-row readout systems are qualitatively identical, with minor differences in the form factors of some parts to fit them into the different cryostats. While a readout platform capable of true 40-row TDM is under development, the 32-row systems only have enough row-address lines to read out 32 distinct SQ1/TES elements per column.

The 32-row systems were made to simulate 40-row TDM readout by reading out each of the 32 physically distinct rows and then repeating measurements on the last physical row 8 times, performing a total of 40 row measurements during a frame. This mode of operation replicates the noise and the timing, which in turn drives the dynamic range, of true 40-row TDM readout. The readout and TES components used were all within ranges specified for X-IFU. These components include SQ1s, SSAs, TESs, and TES shunt resistors [6].

The detectors are NASA LPA 2.5a-style TESs [8] that are baselined for X-IFU. These are 50 μm wide square stripeless TESs consisting of a Mo/Au bilayer with Nb leads. Each has a 240 μm square overhanging Au/Bi absorber. The detectors are arranged in a 32 pixel \times 32 pixel TES array on a 250 μm detector pitch. The detector-bias loop contains a 75 $\mu\Omega$ shunt resistor and 640 nH total loop inductance, as specified for TDM in X-IFU. Since the total loop inductance is roughly 60% of the critical inductance (L_{crit}) when the TES is biased at 11% of its

normal resistance of $R_n = 8.83 \text{ m}\Omega$, the TES pulse response is overdamped.

The maximum number of rows in a TDM system, N , is determined by SQUID dynamic range requirements and the maximum acceptable level of readout noise, which increases as \sqrt{N} due to aliasing [9]. SQUID dynamic range is improved via the operation of each row in a digital flux-locked loop (FLL) [10]. In the FLL, each row's error signal, the deviation in V_{er} from the lock point, is measured and the flux feedback signal necessary to return the SQUID to the lock point is stored for application in the next timing frame. Rapid changes in TES current, such as at the onset of an X-ray pulse, produce a significant error signal. Accurate measurement of TES current relies on the FLL keeping the error signal within a region of the SQUID curve where V_{er} is roughly linear with SQ1 flux. When locked on their steep slope for lowest noise, the SQ1s have a total linear dynamic range of about 0.3 Φ_0 .

The maximum-rising current-slew rate, which occurs at the onset of a pulse, must share the available dynamic range with the maximum-falling current-slew rate, which occurs after the pulse peak. Based on the shape of a critically-damped pulse, we allocate 88% of the dynamic range to the steepest rise and 12% to the steepest fall. The dynamic range allocated to the rise is thus 0.264 Φ_0 and the dynamic range constraints are given by

$$\Delta\Phi = M_{in1} t_{row} N dI/dt|_{max} \leq 0.264 \Phi_0 \quad (1)$$

where $\Delta\Phi$ is the maximum flux offset from the lock point, M_{in1} is the mutual inductance of the SQ1 input coil, t_{row} is the time allocated for each row measurement (the *row time*), and $dI/dt|_{max}$ is the maximum-rising current-slew rate for the highest-energy X-ray of interest, which is 12 keV for X-IFU.

M_{in1} was chosen to meet the dynamic range requirements. An LPA 2.5a TES, biased at 11% of R_n at a bath temperature of 55 mK, has a measured maximum slew rate of 0.262 A/s at 12 keV. Assuming $t_{row} = 160 \text{ ns}$, this sets the maximum allowed M_{in1} at 305 pH. We chose $M_{in1} = 277 \text{ pH}$ to allow for some variation among TESs.

Modifications to the cryostat wiring were needed for TDM to meet X-IFU energy resolution requirements. In previous configurations, coupling between cryostat lines increased the settling time of TDM readout, resulting in degraded energy resolution when $t_{row} = 160 \text{ ns}$ due to increased readout noise and crosstalk. To address these issues, capacitive coupling between cryostat lines was reduced via the addition of ground planes and the effects of coupling were reduced by reversing the polarity of wire bond pairs from the cryostat lines to the SSA and multiplexer chips for better SQUID amplifier stability. These two changes greatly improved the readout noise and crosstalk when the TDM systems were operated with 160 ns row times.

Performance was demonstrated in both single-column and three-column X-ray measurements with $t_{row} = 160 \text{ ns}$. The single-column measurements used SQ1s with 10 μA critical currents, providing a 40-row multiplexed readout noise of 25.6 pA/ $\sqrt{\text{Hz}}$, referred to the TES current. The three-column measurements used the same 10 μA column and two 15 μA SQ1 columns. The two 15 μA columns had an average readout noise of 23.4 pA/ $\sqrt{\text{Hz}}$. The three columns had a yield of

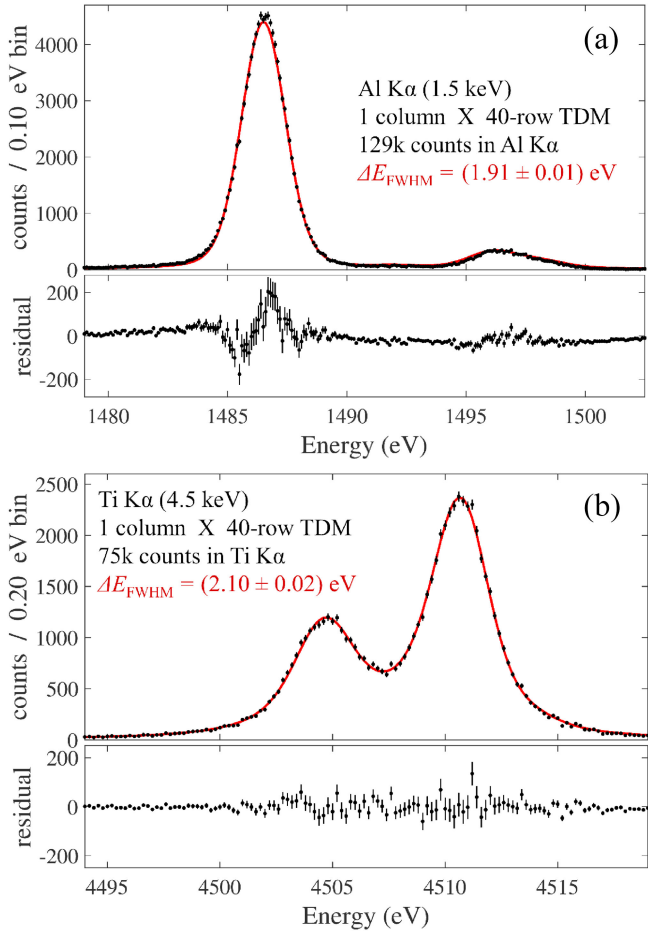


Fig. 2. Single-column 40-row spectra of the lower energy targets. The black dots are histogrammed data and the solid red line is the best fit to data. Residuals are shown below. The uncertainties provided for energy resolution are statistical and do not account for systematic deviations from line models. (a) Combined Al K α spectrum. (b) Combined Ti K α spectrum.

85 good pixels out of 96 pixels. Pixels were flagged as bad for several reasons: two pixels had lower than intended bias loop inductance and thus had leading-pulse-edge current-slew rates that were too fast to track for X-ray energies above 4.5 keV; two pixels had faulty SQ1s with bi-stable lock points that defeated conventional pulse analysis; three pixels had faults in either the TES or interface chip (inductors and shunt resistors) that prevented their TES current from being read out by the multiplexer; and four pixels were otherwise alive but did not respond to X-rays, possibly due to minor misalignment of the tight-fitting Cu aperture. These pixels were excluded from analysis.

III. MEASUREMENTS AND RESULTS

The performance of 40-row TDM was tested with X-ray spectroscopy measurements. X-rays were produced by a tube source that fluoresced high-purity Al, Ti, Mn, and Co foil targets and a crystal of KBr. The input X-ray rate (C_R) to the TES arrays was about 0.5 counts per second (cps) per pixel in all measurements except Al, where it was 0.3 cps.

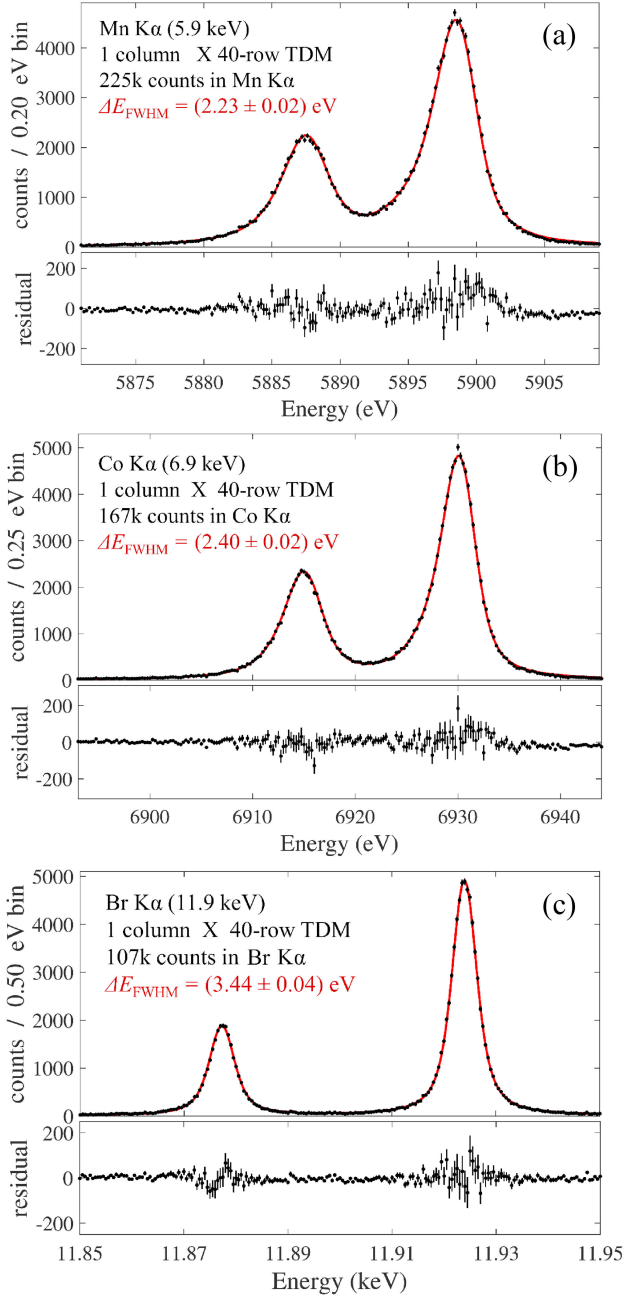


Fig. 3. Single-column 40-row spectra of the three highest energy targets. (a) Combined Mn K α spectrum. (b) Combined Co K α spectrum. X-IFU's main energy resolution specification is at 7 keV. (c) Combined Br K α spectrum. X-IFU's highest energy of interest is 12 keV.

X-IFU has a requirement that 90% of photon events received from a 1.5 cps/pixel source with a Crab-like spectrum must be “high resolution” events, or events that meet the energy resolution requirements listed in this paper. Since this Crab-like source has a mean X-ray energy of 2 keV [11], scaling by X-ray energy ($E_{\text{X-ray}}$) and count rate is necessary to compare this X-IFU requirement to our measurements. Degradation in energy resolution due to crosstalk scales as $E_{\text{X-ray}} \sqrt{C_R}$ [12], where the energy dependence is due to the magnitude of crosstalk scaling linearly with the energy of perpetrator pulses and the $\sqrt{C_R}$

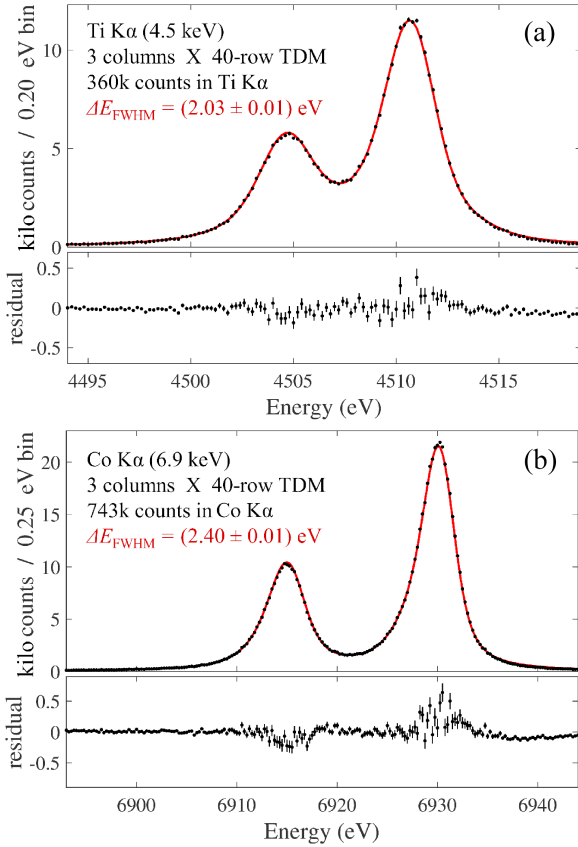


Fig. 4. Three-column, 40-row spectra at two energies. (a) Combined Ti K α spectrum. (b) Combined Co K α spectrum. These multicolumn measurements have similar resolution to the single column measurements in Fig. 2(b) and Fig. 3(b).

dependence is the result of crosstalk from X-ray events behaving as a Poisson point process, similar to shot noise. According to this scaling rule, all of our measurements (except for those of the Al target) should have worse resolution degradation than if they were taken on a 1.5 cps/pixel Crab-like source. From this analysis, we conclude that our measurements more than satisfy the experimental conditions imposed by the X-IFU rate requirement.

The pulse data records were 52.4 ms long (8192 frames) with a pre-trigger fraction of 25%. Pileup cutting removed all records in which more than one X-ray arrived in the same TES. Crosstalk cutting was employed between specific types of perpetrator-to-victim pixel pairs: timing row N to timing row $N + 1$ within a column (time nearest neighbor) and all pixels to all pixels within a column (distant pixel). In addition, the multi-column datasets employed cross-column cutting of victim pixels when the perpetrator pixel was in the same row or within the preceding 5 rows. Each type of crosstalk cutting rejected any X-ray pulse in a victim channel that was coincident with an X-ray pulse in a perpetrator channel within a specified time window: 2 ms wide for distant-pixel cuts, 5 ms wide for cross-column cuts, and the entire 52.4 ms record of the victim pulse for time-nearest-neighbor crosstalk cuts. In all of these 40-row datasets, data cutting for pileup and crosstalk allowed the survival of at least

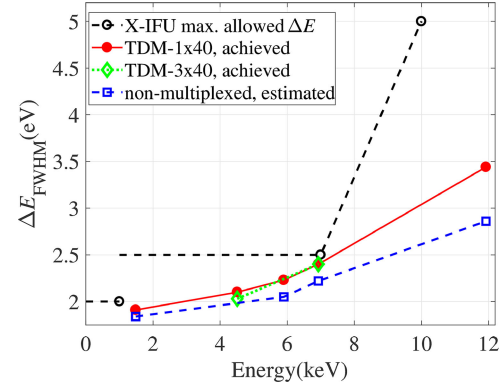


Fig. 5. Energy resolution vs. X-ray energy in the LPA 2.5a TDM-40 data. X-IFU's present resolution requirements are 2.5 eV at 7 keV and 5 eV at 10 keV, with an additional goal of 2.0 eV at 1 keV. The TDM-40 results all lie below this requirements curve. Estimated non-multiplexed resolution was obtained from 4-row TDM measurements, where resolution degradation from multiplexing is low enough to approximate non-multiplexed behavior. The lines between the TDM and non-multiplexed data points are to guide the eye.

90% of the X-ray pulses, which matches requirements for event grading in X-IFU's high-resolution modes.

After cuts were performed, TES data streams were analyzed individually via constrained optimal filtering to obtain pulse heights [13]. Pulse heights were converted into energies using K α and K β lines for calibration, except for Br where K $\alpha 1$ and K $\alpha 2$ were used for calibration. X-ray events from TES rows that were not repeated or flagged as bad were then added to form a single energy histogram as a combined spectrum. Energy resolution was extracted by fitting the combined spectrum to previously measured line shapes [14]–[17].

Pixel uniformity was also studied via fitting to individual TES spectra. The measured energy resolution of individual TESSs in a three-column Co K α measurement had a standard deviation of 0.11 eV. Because the statistical error for each measured individual pixel resolution is 0.10 eV, this indicates excellent pixel uniformity in the three columns.

The combined spectra for one-column measurements are shown in Figs. 2–3 with best-fit resolutions of (1.91 ± 0.01) eV for Al K α , (2.10 ± 0.02) eV for Ti K α , (2.23 ± 0.02) eV for Mn K α , (2.40 ± 0.02) eV for Co K α , and (3.44 ± 0.04) eV for Br K α lines. Three-column measurements for Ti K α and Co K α are shown in Fig. 4, demonstrating that multicolumn performance is comparable to single column performance.

A comparison with X-IFU specifications is shown in Fig. 5. These results meet X-IFU's resolution requirements of 2 eV below 1 keV, 2.5 eV below 7 keV and 5 eV at 10 keV. They also meet X-IFU's 12 keV energy-range requirement.

IV. CONCLUSION

We have demonstrated 40-row TDM readout that meets the energy-range and resolution requirements to be Athena X-IFU's backup readout option. The next step in our development is the construction of a new 40-row, kilopixel-scale TDM system to screen TES arrays for X-IFU and continue to refine TDM readout. When it comes online in the spring of 2019, this will be the largest TES X-ray spectrometer array in the world.

REFERENCES

- [1] J. Uhlig *et al.*, "High-resolution X-ray emission spectroscopy with transition-edge sensors: present performance and future potential," *J. Synchrotron Radiat.*, vol. 22, no. 3, pp. 766–775, May 2015.
- [2] S. R. Bandler *et al.*, "Advances in small pixel TES-based X-ray microcalorimeter arrays for solar physics and astrophysics," *IEEE Trans. Appl. Supercond.*, vol. 23, no. 3, Jun. 2013, Art. no. 2100705.
- [3] D. Barrett *et al.*, "The athena X-ray integral unit (X-IFU)," *Proc. SPIE*, vol. 9905, Aug. 2016, Art. no. 99052F.
- [4] J. Van der Kuur *et al.*, "Optimizing the multiplex factor of the frequency domain multiplexed readout of the TES-based microcalorimeter imaging array for the X-IFU instrument on the Athena X-ray observatory," *Proc. SPIE*, vol. 9905, Jul. 2016, Art. no. 99055R.
- [5] W. B. Doriese *et al.*, "A practical superconducting-microcalorimeter X-ray spectrometer for beamline and laboratory science," *Rev. Sci. Instrum.*, vol. 88, no. 5, Apr. 2017, Art. no. 053108.
- [6] W. B. Doriese *et al.*, "Optimization of Time- and Code-Division-Multiplexed Readout for Athena X-IFU," *IEEE Trans. Appl. Supercond.*, doi: [10.1109/TASC.2019.2905577](https://doi.org/10.1109/TASC.2019.2905577).
- [7] H. H. Zappe, "Josephson quantum interference computer devices," *IEEE Trans. Magn.*, vol. MAG-13, no. 1, pp. 41–42, Jan. 1977.
- [8] A. Miniussi *et al.*, "Performance of an X-ray Microcalorimeter with a 240 μm absorber and a 50 μm TES bilayer," *J. Low Temp. Phys.*, vol. 193, no. 3–4, pp. 337–343, Nov. 2018.
- [9] W. B. Doriese *et al.*, "Progress toward kilopixel arrays: 3.8 eV microcalorimeter resolution in 8-channel SQUID multiplexer," *Nucl. Instrum. Methods Phys. Res. Sect. A*, vol. 559, no. 2, pp. 808–810, Apr. 2006.
- [10] C. D. Reintsema *et al.*, "Prototype system for superconducting quantum interference device multiplexing of large-format transition-edge sensor arrays," *Rev. Sci. Instrum.*, vol. 74, no. 10, pp. 4500–4508, Oct. 2003.
- [11] M. G.F. Kirsch *et al.*, "Crab: The standard X-ray candle with all (modern) X-ray satellites," *Proc. SPIE*, vol. 5898, Aug. 2005, Art. no. 589803.
- [12] R. L. Kelley *et al.*, "The suzaku high resolution X-ray spectrometer," *Publ. Astron. Soc. Jpn.*, vol. 59, no. sp1, pp. S77–S112, Jan. 2007.
- [13] J. W. Fowler *et al.*, "The practice of pulse processing," *J. Low Temp. Phys.*, vol. 184, no. 1–2, pp. 374–381, Jul. 2016.
- [14] C. T. Chantler, M. N. Kinnane, C.-H. Su, and J. A. Kimpton, "Characterization of $\text{K}\alpha$ spectral profiles for vanadium, component redetermination for scandium, titanium, chromium, and manganese, and development of satellite structure for $Z = 21$ to $Z = 25$," *Phys. Rev. A*, vol. 73, no. 1, Jan. 2006, Art. no. 012508.
- [15] G. Hölzer, M. Fritsch, M. Deutsch, J. Härtwig, and E. Förster, " $\text{K}\alpha_{1,2}$ and $\text{K}\beta_{1,3}$ X-ray emission lines of the 3d transition metals," *Phys. Rev. A*, vol. 56, no. 6, pp. 4554–4568, Dec. 1997.
- [16] M. O. Krause and J. H. Oliver, "Natural widths of atomic K and L levels, $\text{K}\alpha$ X-ray lines and several KLL Auger lines," *J. Phys. Chem. Ref. Data*, vol. 8, no. 2, pp. 329–338, Apr. 1979.
- [17] J. A. Bearden, "X-ray wavelengths," *Rev. Mod. Phys.*, vol. 39, no. 1, pp. 78–174, Jan. 1967.